International Journal of GEOMATE, Dec., 2023 Vol.25, Issue 112, pp.56-63
ISSN: 2186-2982 (P), 2186-2990 (O), Japan, DOI: https://doi.org/10.21660/2023.112.g13201
Geotechnique, Construction Materials and Environment

COMPUTATIONAL FLUID DYNAMICS ANALYSIS OF FORCED CONVECTION HEAT TRANSFER THROUGH RECTANGULAR PLATE FIN HEAT SINK

Supachok Chokngamvong[1,2], Jetsadaporn Priyadumkol[1,2], Machimontorn Promtong[1], Kittipos Loksupapaiboon[1,2] and Chakrit Suvanjumrat[1, 2*]

[1]Department of Mechanical Engineering, Faculty of Engineering, Mahidol University, Nakorn Pathom 73170, Thailand;
[2]Laboratory of Computer Mechanics for Design (LCMD), Department of Mechanical Engineering, Faculty of Engineering, Mahidol University, Nakorn Pathom 73170, Thailand

*Corresponding Author, Received: 26 May 2023, Revised: 27 Nov. 2023, Accepted: 28 Nov. 2023

ABSTRACT: This study focuses on developing a computational fluid dynamics (CFD) model for analyzing forced convection heat transfer in a heat sink with straight fins. The heat sink's practical design was considered, and OpenFOAM, an open-source CFD code software, was utilized for the model development. The study identified the SST k-ω turbulence model as suitable for the CFD model and validated its accuracy by comparing results with experimental data, showing an average error of less than 5.19%. The CFD results revealed the full development of the thermal boundary layer in the fin channels, emphasizing its significance for heat transfer performance. Notably, an increase in airflow inlet or Reynolds number was found to gradually enhance the heat transfer performance. The study established correlations between heat sink length, Reynolds number, and heat transfer performance, proposing a novel empirical equation with an average error of less than 4.46%. This equation was deemed a valuable tool for designing straight-fin heat sinks for electronic devices, and the CFD model, similar to this case, could be employed in future OpenFOAM-based studies.

Keywords: Conjugate heat transfer, Forced convection, Plate fin, Heat sink, OpenFOAM

1. INTRODUCTION

Effective heat flux removal from electronic devices plays a crucial role in enhancing performance and prolonging the lifespan of their components. The heat sink serves as a key component in the cooling system, efficiently maintaining low temperatures for electronic devices. Within this system, the convection phenomenon influencing heat transfer in the heat sink can be impacted by laminar, transitional, and turbulent flow. To determine the flow type, the Reynolds number ($Re = UD_h/\nu$) is commonly employed, where U represents flow velocity, D_h is the hydraulic diameter, and ν is the kinematic viscosity. This study specifically focuses on forced convection heat transfer within the Reynolds number range of 20,000 to 100,000, examining microchannel heat sinks with various entrance ducts [1]. The laminar flow equations were applied in this investigation. Other related studies in the laminar flow regime explored microchannel [2] and microchannel pin-fin heat sinks [3], with Reynolds numbers falling within the 100 to 1,000 range.

Simulation studies on heat transfer commonly employ computational fluid dynamics (CFD) software, with previous literature focusing predominantly on natural convection rather than forced convection [4]. In the context of cooling electronic devices, forced airflow parallel to the fins of heat sinks is crucial. The forced convection heat transfer, influenced by fluid heating around the fin surface due to heat transfer across the thermal boundary layer, significantly affects device cooling performance. Exploring the effects of fin geometries on heat transfer in heat sinks is a complex task addressed using CFD. For instance, Chingulpitak et al. [5] utilized ANSYS software to investigate fluid flow and heat transfer characteristics of a heat sink with perforated plate fins, employing various RANS turbulence models. The optimal circular perforation for heat sink fins was determined to be a perforation number of 27 with a diameter of 5 mm. While the elliptical shape of fins presents manufacturing challenges, its performance depends on porosity and representative elementary volume (R.E.V.) [6]. Kewalramani et al. [7] found that low R.E.V. and high porosity contribute to the high thermal performance of micro pin fin heat sinks. Additionally, Chang [8] studied two and three-step plate fins within the Reynolds number range from 5,000 to 40,000, revealing that air velocities increase the convection heat transfer coefficient, reducing thermal resistance. However, the coefficient of two and three-step fins was less than straight plate fins. The most intricate fin shapes of miniature heat sinks were explored by [9], combining different geometries of integral and interrupted straight and wavy fins. Through CFD simulation, they determined that the wavy-wavy-

wavy and straight-straight straight arrangement of fins outperformed other configurations. Despite the potential for increased heat transfer performance through complex fin geometry, the associated manufacturing difficulties and high costs suggest a reconsideration of the straight plate-fin for heat sink design. Moreover, the existing research focused solely on forced convection heat transfer models, resulting in differences between simulation and experimental results. To enhance accuracy and reliability in CFD results, utilizing conjugate heat transfer for modeling forced convection from heat sinks is crucial, and selecting an appropriate turbulence model with a corrected scheme and iterative solution is paramount for a straight fin heat sink within the low Reynolds number range of 1,000 to 10,000. CFD simulations were conducted using the open-source software OpenFOAM [10], specifically designed for simulating forced convection heat transfer [11]. Various heat sink geometries, including the number of fins, fin length, and fin height, were meticulously examined. The empirical findings were utilized to formulate a Nusselt number expression in relation to the Reynolds number and heat sink geometries. The study proposed a novel mathematical model based on conjugate forced convection heat transfer, providing a reliable tool for the design of straight fin heat sinks. This model holds promise for enhancing the efficiency of heat sinks and will be valuable for both users and manufacturers in future applications.

2. COMPUTATIONAL FLUID DYNAMICS MODELING

2.1 Reynolds-Averaged Navier-Stokes

In this study, the chosen working fluid is air, and it is treated as an incompressible and Newtonian fluid. As a result, the governing equations for the forced convection heat transfer flow past the heat sink can be expressed as follows:

$$\frac{\partial \overline{U}_i}{\partial x_i} = 0 \tag{1}$$

$$\frac{\partial \overline{U}_i}{\partial t} + \frac{\partial \overline{U_\iota U_J}}{\partial x_j} = \frac{\partial \bar{p}}{\rho \partial x_i} + \nu \frac{\partial^2 \overline{U}_i}{\partial^2 x_i} - \frac{\partial \overline{\acute{U}_\iota \acute{U}_J}}{\partial x_i} + \bar{S}_i \tag{2}$$

$$\frac{\partial \overline{T}}{\partial t} + \frac{\partial \overline{U_J T}}{\partial x_j} = \frac{\nu}{P_r} \frac{\partial^2 \overline{T}}{\partial^2 x_i} - \frac{\partial \overline{\acute{T}\acute{U}_J}}{\partial x_i} + \bar{q}_f \tag{3}$$

where ρ denotes a fluid density, ν denotes kinematic viscosity, P_r denotes Prandtl number, $\bar{S}_i$ denotes the source term, and $\bar{q}_f$ denotes the heat flux to fluid. $\overline{U}_i$, $\bar{p}$, and $\overline{T}$ denote the time-averaged of velocity component, pressure, and temperature, respectively.

The terms $-\rho\overline{\acute{U}_\iota \acute{U}_J}$ and $-\rho\overline{\acute{T}\acute{U}_J}$ are referred to as the Reynolds stress and turbulent heat flux terms, respectively. These equations represent the Reynolds-averaged Navier-Stokes equations (RANS). The presence of fluctuations in fluid motion leads to the emergence of the Reynolds stress term. Boussinesq introduced a hypothesis for modeling the Reynolds stress as a function of the mean rate of fluid deformation, aiming to account for the fluctuating velocity component [12]. This is expressed in Equation (4).

$$-\rho\overline{\acute{U}_\iota \acute{U}_J} = \frac{1}{3}\delta_{ij}\overline{\acute{U}_\iota \acute{U}_\iota} - \mu_t\left(\frac{\partial \overline{U}_i}{\partial x_j} + \frac{\partial \overline{U}_j}{\partial x_i}\right) \tag{4}$$

where μ_t denotes turbulent viscosity.

The turbulent viscosity is determined through specific equations inherent to RANS turbulence models. In this study, the turbulence viscosity term is addressed using the two-equation transport model known as SST k-ω, which falls under the category of RANS turbulence models.

2.2 Conjugate Heat Transfer

The temperature is determined using the energy equation [13]. In the solid domain, the energy equation is formulated as follows:

$$\frac{\boldsymbol{\partial \overline{T}}}{\boldsymbol{\partial t}} = \frac{\boldsymbol{k}}{\boldsymbol{\rho_s C_p}} \frac{\boldsymbol{\partial^2 \overline{T}}}{\boldsymbol{\partial^2 x_i}} + \boldsymbol{\bar{q}_s} \tag{5}$$

where k denotes the thermal conductivity, ρ_s denotes the solid density, C_p denotes the specific heat capacity of solid, and $\bar{q}_s$ denotes the heat flux to solid.

The heat flux is required to adhere to the conservation of energy at the solid-fluid interface. Consequently, the heat flux in both the solid and fluid domains is considered equal.

$$\bar{q}_f = \bar{q}_s \tag{6}$$

3. COMPUTATIONAL FLUID DYNAMICS DOMAIN

The CFD domain designated for investigating the conjugate heat transfer of the heat sink possesses dimensions of 1,500 mm in length, 800 mm in width, and 800 mm in height, as illustrated in Figure 1. To minimize boundary effects, the heat sink is positioned at a distance of 500 mm from the inlet, and its height from the bottom of the domain is set to 300 mm. In the study, seven inlet flow velocities are employed to achieve Reynolds numbers ranging from 1,000 to 10,000, specifically 2, 4, 6, 8, 10, 14, and 17 m/s. To explore a range of scenarios, the heat input to the bottom surface of the heat sink is varied across four values: 4.71, 7.06, 9.67, and 13.40 Watts. It is important to note that conduction heat transfer is taken into account within the heat sink material, which is composed of aluminum 6063-T5 alloy with a thermal conductivity of 167 W/mK.

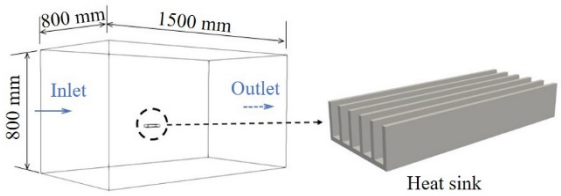

Fig.1 Schematic of conjugate heat transfer domain

3.1 Heat Sink Geometry

The heat sink's fin array, commonly employed in cooling microelectronic devices, is characterized by dimensions derived from the experiments conducted by Adhikari et al. [14]. Specifically, the heat sink has a length, width, height, and thickness of 75, 42, 17, and 2 mm, respectively. Following the validation of the CFD model, the heat sink's geometry is systematically varied to investigate its impact on conjugate heat transfer. The variations in the heat sink's geometry align with practical manufacturing considerations. As a result, this study encompasses a total of 112 simulation cases, with the number of fins held constant due to their minimal influence on the forced convection heat transfer of the straight fin heat sink [14].

3.2 Grid Independence Study

The 3-D computational domain for the conjugate heat transfer analysis of the heat sink is illustrated in the cross-section view in Figure 2. Both the void and heat sink are constructed using 3-D cells, with the heat sink being divided into hexahedron cells. Hexahedron and tetrahedron cells are utilized to construct the void surrounding the heat sink, with hexahedron cells primarily allocated near the heat sink surface for practical fining. Tetrahedron cells are assigned to the void cells adjacent to the hexahedron cells, facilitating an effective cell structure for conjugate heat transfer and enhancing the interaction between the heat sink and airflow. During the CFD simulation validation, the heat sink employs a total of 156,288 cells, while the fluid flow around it utilizes a total of 7,812,237 cells. The 3-D cells of the airflow, in proximity to the heat sink surface, are found to achieve a y+ value of less than 5. The heat sink is also constructed with fined cells, totaling 26,400 cells on the cross-section, ensuring efficient heat transfer from the heat sink to the airflow. An independent grid study is conducted by refining cells near the heat sink surface, featuring four levels of cell numbers (7,750,639; 7,784,871; 7,968,525; and 8,412,624) to determine grid independence. The Nusselt number, employed for testing grid independence, is expressed as follows:

$$Nu = \frac{QD_h}{sHk_f(T_s - T_\infty)} \quad (7)$$

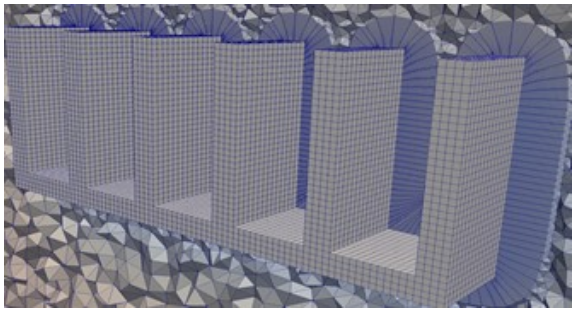

Fig.2 Cell structure of the conjugate heat transfer near the heat sink in the cross-section view

where Nu denotes Nusselt number, Q denotes the heat input, k_f denotes the thermal conductivity of air at film temperature, T_s denotes the fin surface temperature, and T_∞ denotes the inlet air temperature.

The hydraulic diameter (D_h) of the heat sinks is determined using the following equation:

$$D_h = \frac{4sH}{s + 2H} \quad (8)$$

where D_h denotes the hydraulic diameter, s denotes the distance between two fins, and H denotes the height of fins.

The graph in Figure 3 illustrates how the Nusselt numbers vary with the number of cells in a computational fluid dynamics (CFD) simulation. Initially, the Nusselt number remained constant with 7,784,871 cells, indicating that increasing cell count had minimal impact on the CFD results. Optimal results were achieved with 7,968,525 cells, chosen for computational efficiency. This specific cell count was determined by maintaining a y+ value of 3.31 near the heat sink surface, although it remained below 5, characteristic of the laminar sublayer. Despite this proximity, the simulation proved effective for the k and ω wall functions, demonstrating the appropriateness of the chosen cell structure for accurate results in turbulence modeling.

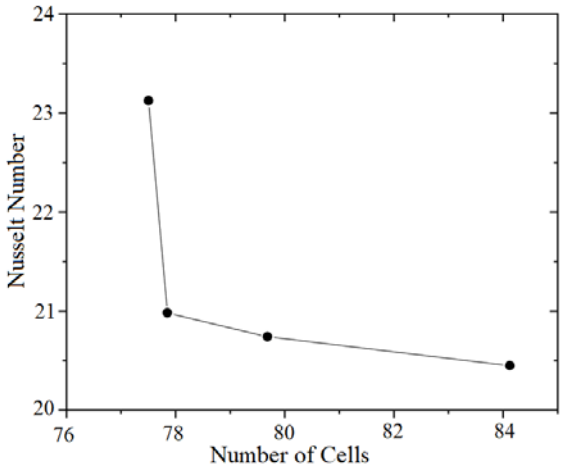

Fig.3 Nusselt number vs. number of cell graph

4. RESULTS AND DISCUSSION

4.1 Validation

A model for conjugate forced convection heat transfer in a rectangular plate-fin heat sink was developed and validated, as depicted in Figure 4, which presents a comparison between experimental and simulated results for this heat transfer phenomenon. The comparison revealed a simulation error, with the CFD simulation exhibiting an average error of less than 5.19%. Notably, the simulation tended to overestimate the surface temperature of the

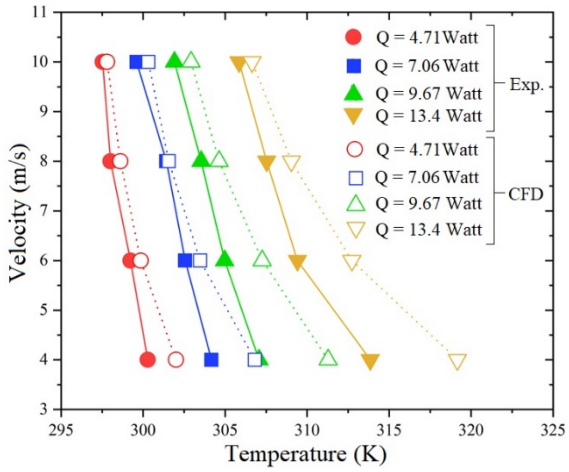

Fig.4 Air inlet velocity vs. temperature graphs of experiment and simulation

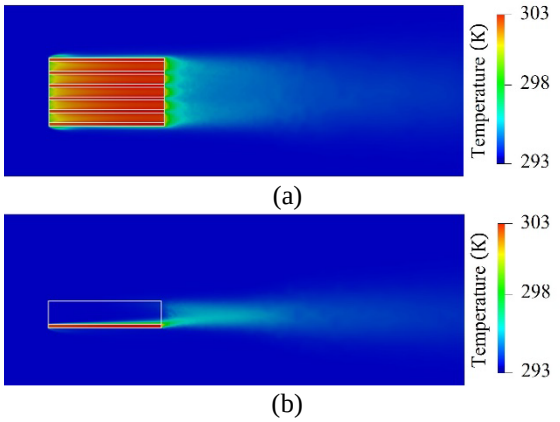

Fig.5 Temperature distribution of the heat sink in (a) top view and (b) front view at mid-section along the fin channel at U∞= 8 m/s and Q = 9.67 W

heat sink. The error was found to be lower at high inlet velocities compared to low inlet velocities, indicating that the chosen cell structure was particularly suitable for high inlet velocities. The color contour illustrates the temperature distribution from the heat sink to the airflow. Figure 5 provides a detailed view of the temperature distribution in the heat sink, with a heat input of 9.67 Watts and an air velocity field of 8.00 m/s. Observing the air temperature, it is evident that the heat sink temperature near the airflow inlet is lower than at the outlet. The air temperature field behind the heat sink exhibits lower temperatures at the top level of the heat sink fins, gradually cooling to the environmental temperature along the length of the heat sink. This region displays turbulent temperature behavior. In the fin channel, heat convection increases at the air outlet, and a boundary layer of air temperature is observed along the length of the fins. Investigating the different temperatures between convective and environmental air temperatures reveals a boundary layer thickness of 5.93 mm. The width of the fin channel was found to have an insignificant impact on the thermal boundary layer, indicating its limited influence on forced convective heat transfer.

4.2 Effects of Heat Sink Geometry

In contrast to prior research where the number of fins did not significantly impact the Nusselt number, this study did not investigate this parameter. The width of the heat sink was deemed insignificant for Nusselt number variations. However, the fin length of the heat sinks was found to notably influence forced convective heat transfer as it directly pertains to the thermal boundary layer. This study explored heat sink lengths ranging from 75 to 200 mm, a range suitable for electric device applications. The CFD results, plotted in Fig. 6 for an input heat of 9.67 Watts, reveal a gradual increase in the Nusselt number with the rise

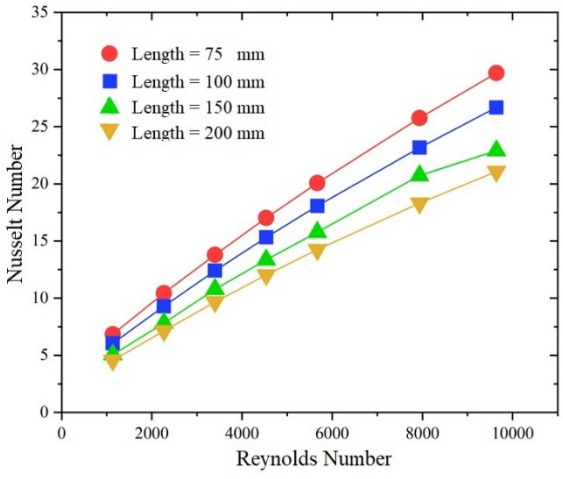

Fig.6 Nusselt number vs. Reynold number graphs of the heat sink with different fin lengths

in Reynolds number. Conversely, the Nusselt number decreases with an increase in heat sink length. The fin length induces an increase in the surface temperature of the heat sink, consequently leading to a gradual reduction in the Nusselt number.

Figure 7 displays the temperature distribution at various heights in the mid-section along the fin channel, considering lengths of 75 mm and 200 mm, with an airflow velocity of 17 m/s and an input heat of 13.4 Watts. Notably, it was observed that the exit temperature in the longer fin channels exceeded that in the shorter ones. This discrepancy was attributed to diminished heat transfer in the longer channels, a consequence of an augmented thermal boundary layer.

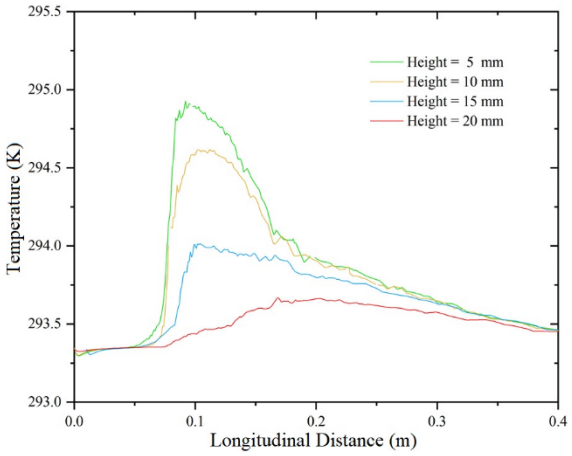

(a)

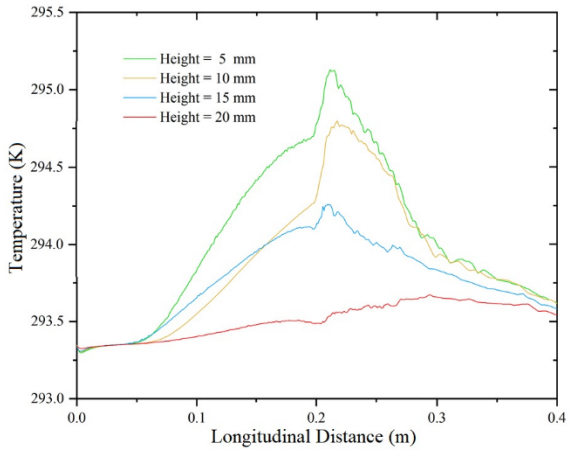

(b)

Fig.7 Temperature distribution at mid-section heights for fin lengths of 75 mm (a) and 200 mm (b) at 17 m/s airflow and 13.4 Watts input heat

4.3 Effects of Input Heat

The Nusselt number serves as a key indicator of the heat transfer efficiency of the heat sink. The observed trend indicates that the Nusselt number increases with higher Reynolds numbers, implying that the velocity of the inlet flow significantly impacts the heat efficiency of the straight fin heat sink. Figure 8 illustrates the effects of the Nusselt number concerning Reynolds number and input heat. As the Reynolds number increases, the Nusselt number gradually rises, signifying the influence of airflow on forced convection heat transfer. Notably, when the Nusselt number falls between 1 and 10, convection is considered laminar, while a range of 100 to 1000 indicates the onset of turbulent convection [15, 16]. This requires the CFD model to be more specific at higher airflow rates. Interestingly, the input heat was found to have an insignificant impact on the Nusselt number, suggesting that the heat source does not significantly affect forced convective heat transfer. As per the Nusselt number formula mentioned earlier, it is evident that heat sink geometry plays a more critical role than input heat. Although the Nusselt number shows minimal variation with changes in input heat in this study, it might have a more pronounced effect at higher input heat levels. Nevertheless, the input heat considered in this study falls within the practical range for heat sinks in electronic devices.

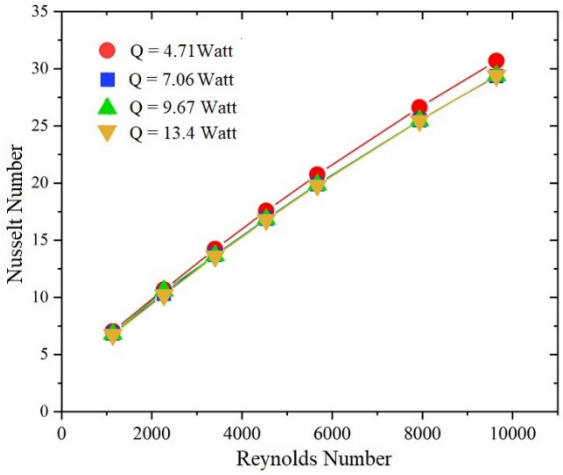

Fig.8 Nusselt number vs. Reynold number graphs of the heat sink with different input heat

4.4 Empirical Modeling

As discussed in the preceding section, the Nusselt number is correlated with both the Reynolds number and the length of the heat sink. The Reynolds number, representing the ratio of inertia forces to viscous forces, is expressed as follows:

$$Re = \frac{\rho V D_h}{\mu} \tag{9}$$

where ρ denotes the fluid density, V denotes the fluid velocity, D_h denotes the hydraulic diameter, and μ denotes the fluid viscosity.

The hydraulic diameter is influenced by the width of the fin channel and the fin height. Consequently, the Nusselt number in forced convective heat transfer is directly related to airflow velocity and heat sink geometry. To model the forced convective heat transfer of the heat sink, the Nusselt number needs to

be expressed as a function of heat sink geometry and air velocity. The Cowper-Symon equation, as employed in [17-20], was applied to describe the relationship between the Nusselt number and Reynolds number for each heat sink length. It is expressed as follows:

$$\frac{Nu(Re,L)}{Nu_{L=0.2}(Re)} - 1 = \left(\frac{L}{D}\right)^{1/P} \quad (10)$$

where P and D denote model constants and L denotes the length of heat sink.

The Cowper-Symon equation is subjected to a logarithmic transformation for analysis.

$$\log\left(\frac{Nu(Re,L)}{Nu_{L=0.2}(Re)} - 1\right) = \left(\frac{1}{P}\right)\log L - \left(\frac{1}{P}\right)\log D \quad (11)$$

Equation (11) is transformed into a linear equation, facilitating the evaluation of constants. The determined values for P and D are -0.0514 and 0.0524, respectively. Through linear regression analysis of empirical data at a heat sink length of 0.2 m, a quadratic equation is obtained and expressed as follows:

$$Nu_{L=0.2}(Re) = -5 \times 10^{-8}Re^2 + 0.0025Re + 1.8318 \quad (12)$$

Equation (12) is inserted into Eq. (10) and subsequently rearranged, resulting in the following equations:

$$Nu(Re,L) = (-5 \times 10^{-8}Re^2 + 0.0025Re + 1.8318)\left(1 + \left(\frac{L}{0.0524}\right)^{1/-0.5214}\right) \quad (13)$$

Equation (13) is introduced to assess forced convective heat transfer in the heat sink, and its validity is tested through comparison with empirical data. Figure 9 illustrates the comparison between empirical data and the novel Nusselt equation for the straight fin heat sink. This equation aligns well with the empirical data, exhibiting an average error of less than 4.46%. It proves to be a satisfactory equation for designing and evaluating the heat transfer performance of straight fin heat sinks. It's essential to note that this equation is limited to Reynolds numbers and heat sink lengths not exceeding 10,000 and 200 mm, respectively. Nonetheless, these limitations are suitable for the heat sinks commonly employed in electronic devices.

5. CONCLUSION

The utilization of conjugate heat transfer in studying the forced convective heat transfer of the heat sink is reasonable and provides several advantages, as outlined below:

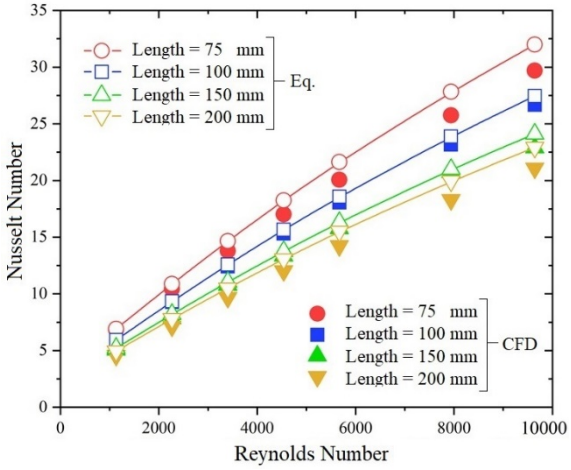

Fig.9 Nusselt number vs. Reynold number graphs of the heat sink with different fin lengths comparing between empirical data and the Nusselt number equation

a) The conjugated forced convective heat transfer of the straight fin heat sink was effectively modeled using the open-source CFD software OpenFOAM. The SST k-ω turbulence model accurately represented the thermal boundary layer in the fin channels, demonstrating good agreement with experimental data. Despite an average error of less than 5.19%, it proved to be a reliable tool for simulating heat transfer phenomena.

b) The length of the heat sink was identified as a significant factor influencing heat transfer performance, with shorter lengths exhibiting better performance compared to longer ones.

c) Higher Reynolds numbers were associated with increased heat transfer performance for straight fin heat sinks, reaching a 300% increase when airflow velocity was raised by 8.5 times.

d) A novel equation for calculating the heat transfer performance of straight fin heat sinks was proposed, exhibiting high accuracy with an error of less than 4.46%. This equation serves as a valuable tool for the design of future straight-fin heat sinks for electronic devices.

The open-source code software, OpenFOAM, employed in this study proves to be an effective tool for developing heat sinks with the SST k-ω turbulence model. The findings suggest that similar CFD models can be successfully simulated using OpenFOAM software in future research.

6. ACKNOWLEDGMENTS

This research received support from the Laboratory of Computer Mechanics for Design (LCMD) within the Department of Mechanical Engineering, Faculty of Engineering, Mahidol University, Thailand.

7. REFERENCES

[1] Moradikazerouni A., Afrand M., Alsarraf J., Mahian O., Wongwises S., and Tran M. D., Comparison of the effect of five different entrance channel shapes of a micro-channel heat sink in forced convection with application to cooling a supercomputer circuit board. Applied Thermal Engineering, Vol. 150, 2019, pp. 1078–1089.

[2] Zhai Y., Xia G., Li Z., and Wang H., Experimental investigation and empirical correlations of single and laminar convective heat transfer in microchannel heat sink. Experimental Thermal and Fluid Science, Vol. 83, 2017, pp. 207–214.

[3] Gupta D., Saha P., and Roy S., Computational analysis of perforation effect on the thermos-hydraulic performance of micro pin-fin heat sink. International Journal of Thermal Sciences, Vol. 163, 2021, pp. 106857.

[4] Saraiya A., Chandramohan V. P., and Bakasubramanian K., Optimization of horizontal rectangular fin heat sink: a CFD with response surface analysis and parametric study. Journal of the Institution of Engineering (India): Series C, Vol. 101, Issue 1, 2020, pp. 149–158.

[5] Chingulpitak S., Ahn, H. S. Asirvatham L. G., and Wongwises S., Fluid flow and heat transfer characteristics of heat sinks with laterally perforated plate find. International Journal of Heat and Mass Transfer, Vol. 138, 2019, pp. 293–303.

[6] Shaeri M. R., and Bonner, R., Heat transfer and pressure drop in laterally perforated-finned heat sinks across different flow regimes. International Communications in Heat and Mass Transfer, Vol. 87, 2017, pp. 220–227.

[7] Kewalramani G. V., Hedau G., Saha S. K., and Agrawai A., Study of laminar single phase frictional factor and Nusselt number in In-line micro pin-fin heat sink for electronic cooling applications. International Journal of Heat and Mass Transfer, Vol. 138, 2019, pp. 796–808.

[8] Chang Y. C., Simulation analysis of heat transfer performance of heat sink with reduced material design. Advance in Mechanical Engineering, Vol. 12, Issue 5, 2020, pp. 1-7.

[9] Hosseinirad E. and Khoshvaght-Aliabadi M., Proximity effects of straight and wavy fins and their interruptions on performance of heat sinks utilized in battery thermal management. International Journal of Heat and Mass Transfer, Vol.173, 2021, pp. 121259.

[10] Chaichanasiri, E., and Suvanjumrat, C., Simulation of three dimensional liquid-sloshing models using C++ open source code CFD software. Kasetsart Journal (Natural Science), Vol. 46, Issue 6, 2012, pp. 978–995.

[11] Suvanjumrat, C., Implementation and validation of OpenFOAM for thermal convection of airflow. Engineering Journal, Vol. 21, Issue 5, 2017, pp. 225–241.

[12] Loksupapaiboon, K., and Suvanjumrat, C., Forced convective heat transfer and fluid flow past a rotating hand-shaped former for improving rubber glove curing. Case Studies in Thermal Engineering, Vol. 47, 2023, pp. 103050. https://doi.org/10.1016/j.csite.2023.103050

[13] Laitinen A., Saari K., Kukko K., Peltonen P., Laurila E., Partanen J., and Vuorinen V., A computational fluid dynamics study by conjugate heat transfer in OpenFOAM: a liquid cooling concept for high power electronics. International Journal of Heat and Fluid Flow, Vol. 85, 2020, pp. 108654.

[14] Adhikari R. C., Wood D. H., and Pahlevani M., An experimental and numerical study of forced convection heat transfer from rectangular fins at low Reynolds numbers. International Journal of Heat and Mass Transfer, Vol. 163, 2020, pp. 120418.

[15] Suvanjumrat, C., Comparison of turbulence models for flow past NACA0015 airfoil using OpenFOAM. Engineering Journal, Vol.21, Issue 3, 2017, pp. 207-221.

[16] Loksupapaiboon K., and Suvanjumrat C., Effects of flow and heat transfer around a hand-shaped former. Engineering Applications of Computational Fluid Mechanics, Vol. 16, Issue 1, 2022, pp. 1619-1640.

[17] Suvanjumrat, C., and Puttapitukporn, T., Determination of drop-impact resistance of plastic bottles using computer aided engineering. Kasetsart Journal (Natural Science), Vol. 45, Issue 5, 2011, pp. 932-942.

[18] Chokngamvong, S., and Suvanjumrat, C., Study of drying kinetics and activation energy for drying a pineapple piece in the crossflow dehydrator. Case Studies in Thermal Engineering, Vol. 49, 2023, pp. 103351. https://doi.org/10.1016/j.csite.2023.103351

[19] Phromjan J., and Suvanjumrat C., Non-pneumatic tire with curved isolated spokes for agricultural machinery in agricultural fields: Empirical and numerical study, Heliyon, Vol. 9, 2023, pp. e18984.

https://doi.org/10.1016/j.heliyon.2023.e18984
[20] Phromjan J., and Suvanjumrat C., Effects on Spoke Structure of Non-Pneumatic Tires by Finite Element Analysis, International Journal of Automotive Technology, Vol. 23, Issue 5, 2022, pp. 1437-1450.